

Wide-Gap Perovskites for Indoor Photovoltaics

Gregory Burwell,* Stefan Zeiske, Pietro Caprioglio, Oskar J. Sandberg, Austin M. Kay, Michael D. Farrar, Yong Ryun Kim, Henry J. Snaith, Paul Meredith,* and Ardalan Armin*


Organic–inorganic halide perovskite semiconductors have revolutionized next-generation photovoltaics (PV) due to several characteristics such as solution-processability, gap tunability, and excellent charge generation and transport properties. This has made them very adaptable for various applications in light harvesting and photodetection. One such rapidly growing application is indoor photovoltaics (IPV) which have the potential to power standalone Internet of Things devices. IPV requires wider optimal bandgaps than solar cells (1.8 vs 1.3 eV) due to the differences between the spectra of artificial lights versus solar radiation. For IPV applications, the active layer wide-gap perovskite must be developed systemically considering all other components of the device, such as interlayers, electrodes, and scaling. This perspective provides an overview of the potential and challenges facing perovskite-based IPV from a theoretical, material, and experimental perspective. Furthermore, accurate characterization of perovskite IPV under simulated indoor conditions is discussed and candidate perovskite PV (PPV) systems are presented to provide insight into IPV development. These include IPV-optimized formamidinium cesium-based perovskite, wide-gap p-i-n devices, and 2D perovskite devices, tested under spectrophotometrically calibrated LED illumination at various indoor-relevant illuminances and benchmarked against thermodynamic predictions. Finally, strategies required to create stable, optimized PPV devices for indoor applications are discussed.

1. Introduction

The proliferation of low-power networked devices, driven by advancements in sensing, electronics, communication protocols, and machine learning (ML), is poised to significantly impact society and various industries through the Internet of Things (IoT).^[1–6] This emerging technology class has the potential to bring about a similar level of disruptive change as other transformative technologies in recent history, such as the smartphone. As the use of IoT devices becomes increasingly prevalent in our homes and workplaces, we must understand their potential environmental and social impacts. Even though individual devices may consume relatively small amounts of power, the cumulative energy consumption and environmental impact from batteries to power IoT devices must be considered as a detrimental scaling effect.^[7] Thus, energy harvesting methods, which generate power for the device from its local environment with minimal and lifelong battery storage requirements, are an ideal solution for low-power IoT applications. Not only does this help to reduce the environmental footprint of IoT devices by reducing their reliance on nonrenewable

G. Burwell, S. Zeiske, O. J. Sandberg, A. M. Kay, Y. R. Kim, P. Meredith, A. Armin
Sustainable Advanced Materials (Sêr-SAM)
Centre for Integrative Semiconductor Materials and Department of Physics
Swansea University
Singleton Park, Swansea SA2 8PP, UK
E-mail: g.burwell@swansea.ac.uk; paul.meredith@swansea.ac.uk; ardalan.armin@swansea.ac.uk

S. Zeiske
Department of Chemistry
Northwestern University
2145 Sheridan Rd, Evanston, IL 60208, USA

 The ORCID identification number(s) for the author(s) of this article can be found under <https://doi.org/10.1002/solr.202400180>.

© 2024 The Authors. Solar RRL published by Wiley-VCH GmbH. This is an open access article under the terms of the Creative Commons Attribution License, which permits use, distribution and reproduction in any medium, provided the original work is properly cited.

DOI: 10.1002/solr.202400180

P. Caprioglio, M. D. Farrar, H. J. Snaith
Department of Physics
University of Oxford
Clarendon Laboratory
Parks Road, Oxford OX1 3PU, UK

O. J. Sandberg
Physics
Faculty of Science and Engineering
Åbo Akademi University
Turku 20500, Finland

Y. R. Kim
Solar Energy Research Institute of Singapore (SERIS)
National University of Singapore (NUS)
Singapore 117574, Singapore

sources of energy, but it also leads to a decrease in the consumption of critical elements used in batteries, which in turn conserves increasingly rare raw materials. Additionally, using self-powered devices can also lower the costs associated with deploying IoT infrastructure, such as installation and maintenance.

Indoor lighting levels have been shown to be typically sufficient to power emerging IoT devices,^[8] and the development of indoor photovoltaics (IPV) is being further advanced by progress in efficient charge controllers and supercapacitors.^[9] This also makes IPV a viable option for powering IoT devices when illumination is not continuous. Operating in a variety of environments, IPVs face different challenges to those of solar cells with some technological considerations for IPV being less complex than those for outdoor photovoltaics. For example, the lower levels of light and milder conditions typically encountered in indoor environments can help to increase the longevity of the devices. They however require more efficient control circuitries since they operate at lower voltages compared to solar cells, plus have more complex requirements for power, voltage, and current matching into the recipient device.

Other aspects of IPV differentiating them from solar cells are the different emission spectra of indoor and sunlight, and the irradiance levels, which set new limits for optimum materials and device parameters. In general, indoor light spectra (predominantly light-emitting diode (LED) lights) are spectrally centered at higher photon energies than sunlight and the spectral peaks are narrower. This means that the optimal bandgap and corresponding predicted power conversion efficiency (PCE) expected for single junctions are generally higher for IPV devices.^[10,11] The radiative thermodynamic PCE limit can be over 50% for typical indoor spectra.

However, to achieve optimal PCE values, IPVs require optical gaps around 1.7–1.9 eV – considerably wider than typical solar photovoltaics (PV) materials such as crystalline silicon (1.1 eV), gallium arsenide (1.42 eV), and cadmium telluride (1.44 eV). This is the primary driving force motivating the development of wide-gap next-generation PV materials for IPV use. In addition, solution-processable PV materials have several attributes that make them desirable for such applications, including mechanical flexibility, low embodied manufacturing energy, and the fact that they are amenable to fabrication techniques like blade-coating and roll-to-roll printing. Organic semiconductors with optical gap tuneability have shown promise, although large nonradiative (NR) losses make it currently impossible to approach the radiative PCE limit. Perovskite semiconductors, in contrast, with higher performance and lower NR losses are of significant technological relevance for indoor applications since they share many of the same desirable features as organic semiconductors.^[3,5,12]

The requirement for wide-gap perovskites for perovskite/silicon tandem solar cells has driven insensitive research.^[13–15] This is a promising approach for surpassing the maximum single-junction performance for conventional outdoor PV. Recent solar-to-electrical PCEs greater than 33% demonstrated in perovskite/Si tandem cells have been achieved by fine-tuning the wide-gap perovskites and spectrally matching them with silicon subcells as well as engineering the interlayers.^[13,16] This has driven fine optimization of the charge-selective interlayers at the electrodes, commonly referred to as the

electron (ETLs) and hole-transporting layers (HTLs). These include the development of self-assembled monolayers (SAMs) such as Me-4PACz ([4-(3,6-dimethyl-9H-carbazol-9-yl)butyl]phosphonic acid).^[13] Device optimization strategies for wide-gap perovskite PV (PPV) materials and associated interlayers as used in single-junction or tandem solar cells offer a promising starting point for IPV applications and a substantial amount of existing knowledge is at hand to be readily employed to perovskite IPVs. However, these materials and devices must be re-evaluated for their use under irradiances typically found indoors including accurate characterization.

Even though an efficiency testing standard for indoor light (IEC TS 62 607-7-2:2023) was published recently, comparing current IPV reports can be still fraught with difficulty since figures of merit, such as PCE, are (at the time of writing) often measured under different spectra and irradiances. However, it is expected that the IPV measurement standard will be adopted by the international PV community, fostering the development and optimization of IPV materials and devices as various loss mechanisms may dominate at different intensities. For example, at very high irradiances, series resistances will dominate the electrical losses, while at low irradiances, shunt resistances will limit the device's performance.^[8] Being able to measure the device under a range of irradiances can help identify the dominant loss mechanisms and inform optimization strategies for IPV development.^[17]

The operating conditions of a real-world IPV device can be extremely variable. One recent study investigating the availability of light for energy harvesting applications reported illuminances between 100 and 3000 lux recorded in different scenarios on the same university campus.^[9] To enable continuous real-world use, an IPV-enabled IoT device should be benchmarked with a similarly broad range of lighting conditions to account for this. To hasten the development of IPV devices and materials, the breadth of possible lighting scenarios must be realistically represented. To this end, the accurate characterization of IPV devices is an area of increasing research attention, with recent reports outlining the influence of experimental factors such as illumination masks, beam homogeneity, stray light, and spectral verification.^[18,19]

In this perspective, we demonstrate the potential of wide-gap PPV devices for IPV applications. We review the theoretical limits of single-junction PV devices under typical indoor lighting conditions and examine the challenges of developing efficient IPVs. Furthermore, to exemplify common bottlenecks in device performance and examine exemplary devices including IPV-targeted formamidinium (FA) cesium-based perovskite, wide-gap p-i-n devices, and 2D perovskite devices are used as models. These are tested under spectrophotometrically calibrated LED illumination at a range of indoor-relevant illuminances. We estimate the radiative and NR losses for PPV devices and attribute the main performance losses to trap-assisted recombination. We also utilize drift-diffusion simulations to estimate the theoretical performance of an IPV-optimized PPV device under varying trap-assisted recombination scenarios. To contextualize these results, IPV performance estimates from literature-derived data are compared under standardized illumination conditions. Finally, we provide an open-source computational tool that applies the technique described by Kay et al. (which uses external quantum efficiency (EQE) spectra and open-circuit voltage (V_{oc}))

measurements under AM1.5G) to estimate the performance of IPV under arbitrary light sources at any illuminance.^[20] Especially in light of the recently published indoor characterization standard protocol, this tool is particularly useful for providing benchmark performance metrics that experiments may be compared with.

2. Spectral Standardization for Efficiency Comparison

Derived from the principle of detailed balance, the trade-off between the absorbed flux of photons and the photovoltage is generated by a single junction solar cell versus bandgap results in an upper, thermodynamic limit of device performance.^[10] In the ideal case, this detailed balance limit is based on an absorption model which assumes the photovoltaic external quantum efficiency (EQE_{PV}) of the device to be given by a unit step function centered at the bandgap. It is usually calculated using the AM1.5G spectrum, as this is the common standard used in solar photovoltaic research (i.e., 1 Sun, **Figure 1a**, green plot). However, if other light spectra, such as those of indoor lighting, are considered, the limit must be recalculated accordingly.

Establishing standard spectra for different lighting conditions, such as those of indoor sources (e.g., IEC TS 62 607-7-2:2023

efficiency testing report under indoor light), would be extremely useful for several reasons. First, it would allow researchers to compare the efficiencies of photovoltaic systems more accurately, as they would all be tested under the same set of conditions. Second, it would enable manufacturers to optimize their products for a particular spectrum, making them more efficient and cost-effective. Finally, by providing a standard for comparison, it would allow for a more accurate calculation of the detailed balance limit of photovoltaic device performance, facilitating the optimization of PPV for different spectra.

To this end, it is useful to calculate the detailed balance limit for a “standard illuminant”, for example, those specified by the International Commission on Illumination (CIE), and then calculate the resultant spectral mismatch (or deviation) of a given laboratory light source from this spectrum.^[21–23] Standard illuminants are defined for typical artificial light sources, including incandescent, fluorescent, and LED sources. An example of a typical phosphor-converted blue LED source is the LED-B4 spectrum, with a correlated color temperature of 5109 K. As it is more common to discuss the “magnitude” of an indoor light source in terms of illuminance, the spectral irradiance can be calculated at a convenient illuminance value (e.g., 1000 lux, see the Supporting Information for details).

Figure 1a shows the normalized CIE LED-B4 spectrum plotted as a function of photon energy and compared to the normalized

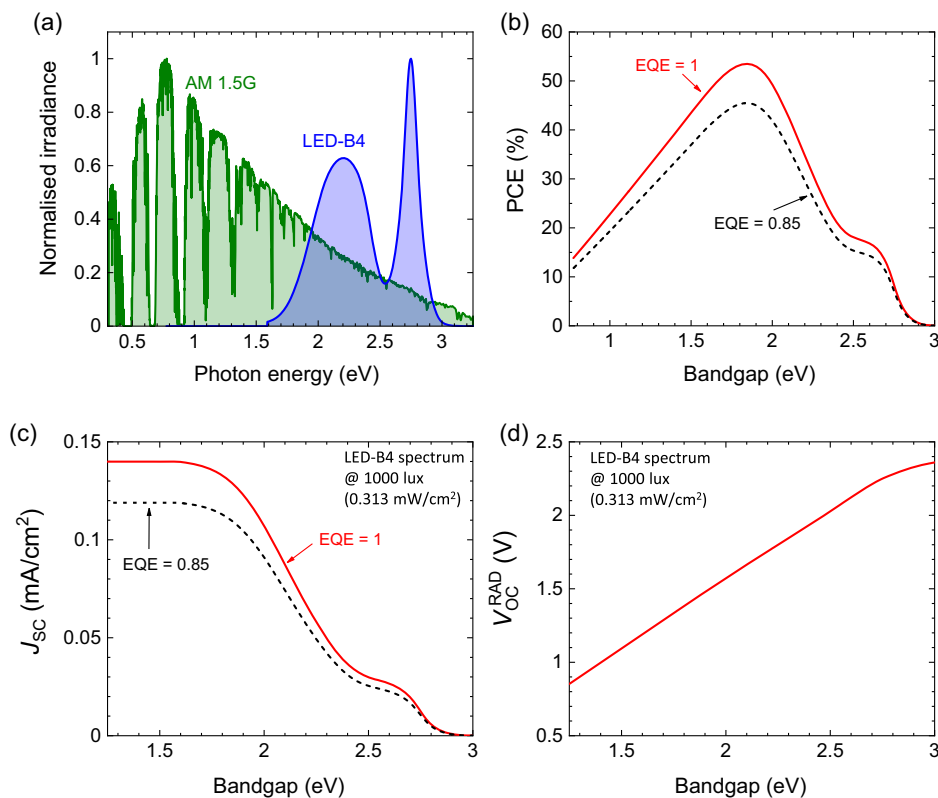


Figure 1. a) Normalized irradiance of a CIE LED-B4 (blue) spectrum for indoor light and standard AM 1.5G spectrum for sunlight (green) plotted as a function of photon energy. b) PCE, as simulated for the LED-B4 spectrum at 1000 lux illuminance (or, 0.313 mW cm⁻²), plotted as a function of bandgap energy, and compared for a maximum above-gap EQE of 1 (red solid line) and 0.85 (black dashed line). c) Repetition of panel (b), but short-circuit current density (J_{sc}) plotted against the bandgap energy. d) Repetition of panel (b), but with the radiative limit of open-circuit voltage (V_{OC}^{RAD}) plotted against the bandgap energy.

AM1.5G spectrum (green). Note that the CIE standard LED-B4 spectrum, as specified in the IEC TS 62 607-7-2:2023 indoor light testing report, is close to our exemplary IPV test apparatus discussed in the following section (see Figure S3, Supporting Information). The predicted thermodynamic PCE limits under indoor conditions emulated by an LED-B4 spectrum at 1000 lux (0.313 mW cm^{-2}) are exemplified in Figure 1b. In this regard, the PCEs were calculated for the radiative limit from detailed balance,^[24] while assuming a step-function EQE_{PV} with an above-gap EQE_{PV} of either unity (red solid line in Figure 1) or more realistically 0.85 (black dashed line in Figure 1). The corresponding short-circuit current density (J_{sc}) and radiative limit of the open-circuit voltage ($V_{\text{oc}}^{\text{RAD}}$) are shown in Figure 1c,d, respectively.

The upper limit of the efficiency can be calculated for more realistic cases where experimental EQE spectra are used which include tail states as opposed to an abrupt onset. Combined with the experimental AM1.5G-corresponding V_{oc} , all J - V parameters can be estimated for indoor conditions. Such an approach is discussed in detail by Kay et al. including the effects of energetic disorder, state-filling, and Urbach tails.^[20] A simplified version of this approach, as used in this work, is provided in an open-source computational code in the Supporting Information. The values obtained from this extrapolation method from EQE and experimental AM1.5G-corresponding J - V parameters can be used as upper-limit benchmark values to minimize the danger of experimental errors in the absence of a measurement protocol.

3. Fabrication of Perovskite Photovoltaics with Tuneable Bandgap

Perovskites in general refer to materials with a crystal structure given by the formula ABX_3 . Of particular relevance to photovoltaics has been the discovery and development of lead halide perovskites; most notably, methylammonium lead iodide (MAPbI_3) and its variants, and more recently lead-free halide perovskites. These perovskite materials exhibit an energy gap tuneability in the range of 1.3–3.1 eV by halide substitution and composition altering making them promising candidates for use in IPV applications. As such, the use of halide perovskites for IPV has been the subject of recent research, which highlights the tunability of the composition as a significant advantage for perovskite IPV.^[2,3,25–34] Figure 2 compares the solar cell performance of reported PPVs under artificial AM1.5G conditions as a function

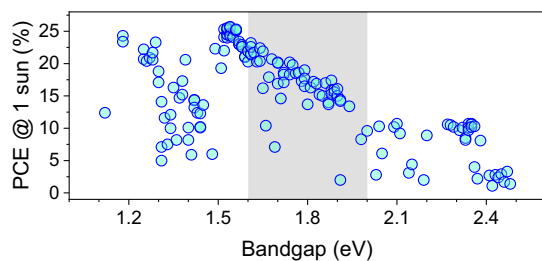


Figure 2. Summary of PCEs of single-junction perovskite devices under AM 1.5G conditions with varying bandgaps reported in the literature. (Adapted from,^[16] which uses bandgap values determined from the first derivative of the EQE). Systems relevant to indoor applications are shaded in grey.

of their bandgaps. Note that comparing the bandgap of PPV materials across the literature can lead to inconsistencies. Here, we use values determined from the first derivative of the EQE spectrum as this is the closest approximation of the energy of the step-function bandgap.^[16]

The advancement of perovskite IPV devices extends beyond the perovskite semiconductor (active) layer, and the constituent parts of the device must be considered.^[31,35–40] The optimization of wide-gap perovskite PV devices requires optimization of the charge-selective transport layers in the PV device, to avoid or minimize energetic misalignment and recombination at the interfaces.^[41,42] The use of SAMs and interlayer choice may have additional implications for device stability.^[43–45] As series resistance-related losses are lower in IPV devices compared with solar cells,^[8] novel transparent conductive electrode structures that are otherwise not suitable for solar cells can be considered. Avoiding transparent oxides that are processed at high temperatures can have additional benefits to IPV device architectures, such as improved device flexibility. The incorporation of metallic grids with transparent polymers has been outlined as a facile approach to this end.^[46,47]

Typical (3D) PPV materials are known for their high PCEs when employed as perovskite solar cells (PSCs), but their practical applications are still limited due to their instability. In contrast, 2D perovskites consisting of an inorganic metal halide layer sandwiched between large hydrophobic organic cations exhibit significantly improved stability against thermal, chemical, and environmental factors.^[48] Subsequently, these 2D perovskite materials have been used as the surface passivator over a 3D perovskite absorber (2D/3D PSCs), making them a promising choice for the future development of PPV.^[49–54] These structures as indoor light absorbers have not yet seen widespread development or been fully optimized for IPV despite having an easily adjustable bandgap from 1.7 to 2.4 eV in 2D perovskite and excellent stability. The primary challenge is the attainment of a uniformly distributed phase with vertical orientation which impacts the charge transfer and the collection efficiency of photogenerated carriers. Therefore, recent research efforts have been dedicated to achieving a phase-pure 2D perovskite layer with vertical orientation through compositional and/or solvent engineering (see Table S2, Supporting Information).^[50,55–57]

The solution-processability of perovskites has been exploited to produce novel device types that include storage elements. Previous reports on the use of perovskites to create photocapacitors outline a promising direction for the use of perovskites for indoor energy harvesting.^[58] Although the low energy density of these structures is a drawback for solar cell applications, this is not as determinantal for IPV applications. The monolithic integration of a mixed-cation mixed-halide PSC with a gel electrolyte-type supercapacitor has been demonstrated in a three-electrode configuration with an overall photoelectrochemical energy conversion efficiency of 11.5%.^[59]

4. Characterization under Indoor Conditions

Measuring the spectral irradiance of a light source accurately is technically challenging and care should be taken when comparing results between laboratories under arbitrary indoor lighting

conditions. Ideally, a spectroradiometer would be used to calibrate the measurement apparatus at the device under test (DUT) location. However, this may not be practical for PV-focused research groups. Instead, one may calculate the spectral irradiance by measuring the spectral shape and total irradiance separately, using equipment that is typically found in research laboratories. The details of the calibration using this method are described in further detail in Supporting Information Section B–C.

To confirm the calibration of an IPV characterization system, it is necessary to measure reference devices with known responsivity.^[60] The appropriate reference device(s) should be selected with care. If photodiodes are used with areas much smaller than that of the DUT, this may lead to inaccuracies in the estimation of total irradiance to the DUT. However, if bus-barred reference cells are used, their absolute $E_{QE_{PV}}$ may be difficult to measure. In practice, it is advisable to measure several reference devices at the DUT location to minimize the overall uncertainty.

When measuring J – V curves, perovskite PV devices are known to exhibit hysteresis commonly attributed to mobile ion migration.^[61,62] It has been shown that the measured PCE can be affected by the scan speed used for the measurement. Further, degradation processes have been shown to have a dependence on the total irradiance.^[63] These two effects point to the scan speed of perovskite PV characterization being an important experimental variable when determining IPV performance; its ideal value may vary as a function of irradiance. Under conditions where slow scan speeds are preferable, the short-term temporal instability of the light source should be considered to reduce experimental uncertainty associated with long measurement times. Another approach may be the development of maximum power point (MPP)-tracking approaches for indoor characterization, equivalent to those demonstrated for PSC measurements.^[64] While research groups have reported perovskite stability based on MPP tracking,^[65–67] there is still a lack of standardized MPP tracking testing protocols for solar cells in general, and indoor conditions in particular (note that the recently published IEC TS 62 607-7-2:2023 efficiency testing report under indoor light does not specify requirements for MPP tracking).^[68] As such, further investigations of the origin and nature of hysteretic behavior, light soaking effects, and ion contribution in PPV are necessary and need to be taken into account when developing corresponding standardized testing protocols. In this regard, Saliba et al. recently reported a systematic discrepancy between short-circuit current values obtained from J – V curves under artificial AM 1.5G conditions and those derived from integrated EQE spectra.^[69] Importantly, this discrepancy was found to be independent of perovskite composition and device architecture clearly highlighting the need for re-evaluating existing standards and developing new testing protocols.

5. Investigation and Development of PPV in Silico

The remarkable rise of perovskites among emerging PV has left in their wake an incredible volume of research output. With over 19 000 articles reported in the Web of Science, identifying suitable approaches to perovskite IPV would be a herculean task if all PSC reports were to be reinterpreted for IPV use separately, and

thus a standardized dataset would be preferable. Fortunately, this endeavor is already underway, with an open-access database and analysis tool for PSCs based on findable, accessible, interoperable, and reusable data principles available to researchers.^[70,71] Utilizing large datasets such as these provides incalculable insights into systems development, especially when combined with ML-based models.^[72,73]

The identification of suitable IPV systems from the myriad of PSC reports (where devices have been measured under AM1.5G conditions) is more straightforward when the reports include accurately measured $E_{QE_{PV}}$ spectra. By integrating over these spectra, one can estimate their expected short-circuit current densities, open-circuit voltages (in the radiative limit), and the open-circuit voltage losses, with the latter determined from the open-circuit voltage under AM1.5G conditions (see Supporting Information). As we explore shortly, extrapolating such NR losses to indoor settings for many PV systems can provide valuable insight into which are most suitable for IPV applications. The use of large datasets and ML can also assist the development of large-area processing techniques.^[74–76] Combined with in-line data such as photoluminescence (PL) imaging of PPV systems, ML has been used to provide insight into large-area fabrication processes.^[77] As IPV device performance is highly sensitive to the (specific) shunt resistance, the use of ML models could provide further insight into fabrication-related shunt formation that will determine the overall performance of IPV modules.^[8]

One-dimensional drift-diffusion (DD) device models have been frequently used in the past to describe the electrical behavior of PPVs.^[78–80] These models are generally based on an effective medium approach describing the charge transport and recombination of electrons and holes in the device, while accounting for space charge effects and interface-related phenomena at interlayer and /or electrode contacts. DD models serve as valuable tools for obtaining an increased understanding of device physics, identifying and investigating loss mechanisms, and guiding device optimization. For example, DD models have been successfully applied to investigate the influence and contribution of transport, trap-assisted recombination, and mobile ions on the device performance in PPVs.^[17,62,78–82] Combined with “big data” approaches, in silico investigation into new approaches to perovskite IPV can reduce the environmental impacts associated with materials discovery and iterative experimentation.^[83]

6. Exemplification and Measurement of an IPV System with Optimized Bandgap

We investigated FA cesium-based perovskite, $FA_{0.85}Cs_{0.15}Pb(I_{0.6}Br_{0.4})_3$, wide-gap p-i-n (“inverted”) devices, utilizing Phenyl- C_{61} -butyric acid methyl ester (PCBM) as the ETL and the SAM Me-4PACz as the HTL. The development of the latter is described in a recent work.^[13] To improve the wetting of the perovskite on top of the SAM, a highly diluted solution of Al_2O_3 nanoparticles was used as an interlayer. To reduce the interface recombination losses between perovskite and ETL, the surface of the perovskite was treated with Imidazolium-Br, following the approach reported in a previous work.^[42]

For examining the performance of the perovskite photovoltaic cell under indoor light conditions, a custom IPV characterization

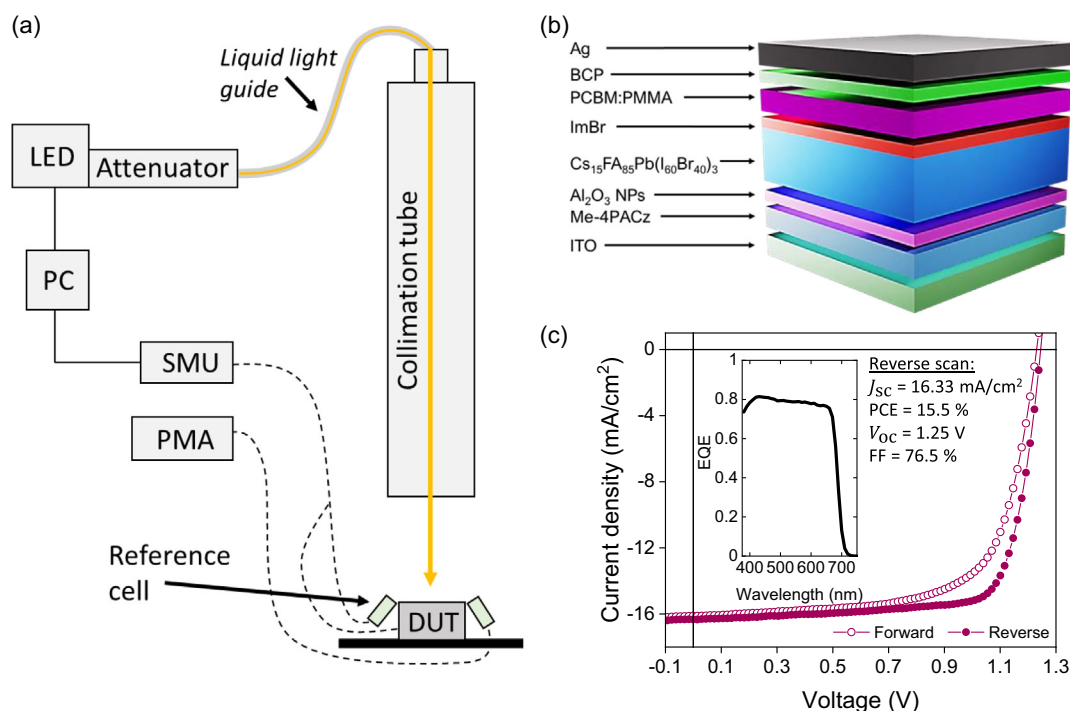


Figure 3. a) Schematic of the IPV characterization setup, where a 4000 K LED with variable output power and LED stabilization in combination with a motorized attenuator is used to stepwise attenuate the incident light intensity. Prior to guiding the output light on the DUT, a liquid light guide is used to fetch the LED light into the collimation tube. A source-meter-unit is used to record the DUT current density versus applied voltage (J - V) curves. For initial light calibration, a NIST-calibrated Luxmeter and silicon photodiode sensor are used as reference devices. b) p-i-n-type device architecture of a wide-gap $\text{FA}_{0.85}\text{Cs}_{0.15}\text{Pb}(\text{I}_{0.6}\text{Br}_{0.4})_3$ PPV treated with ImBr and with Me-4PACz as a HTL. c) J - V curve under artificial solar illumination (AM 1.5G) of a $\text{FA}_{0.85}\text{Cs}_{0.15}\text{Pb}(\text{I}_{0.6}\text{Br}_{0.4})_3$ PPV with SAM + ImBr measured in forward (open symbols) and reverse (closed symbols) scan directions. Photovoltaic performance parameters are indicated in the plot. The inset shows the EQE_{PV} plotted as a function of wavelength.

apparatus was used (see Figure 3a). The setup comprises a 4000 K LED (Prizmatix, UHP-T-LED-White) as a light source. To illuminate the DUT, a liquid light guide from Prizmatix was employed to transmit the attenuated probe light from the light source to a collimator, which was directly affixed to a collimation tube. Note that the recently published IEC TS 62 607-7-2:2023 standard does not specify the use of diffuse or collimated light sources for indoor testing, but rather specifies an angular correction factor. As such, this is an experimental decision for the test facility reporting IPV performance under this standard.

The question of whether to benchmark IPV devices under collimated or diffuse light can be viewed as a balance between experimental reproducibility and a realistic representation of indoor lighting scenarios. In this regard, we found that the relative error introduced by collimated light testing can be considered more controlled and predictable than its diffuse counterpart (see Supporting Information, Section E). A combination of black DUT illumination masks and black shielding around the whole IPV testing apparatus was used to minimize parasitic stray light. The light intensity was varied through a combination of controlling the LED power driving current and a two-prism attenuator from Standa. For the initial light power calibration, a NIST-calibrated silicon reference photodiode from Newport (818-UV) was used, while the light intensity dependent output spectra of the IPV light source were recorded manually using a Hamamatsu photonic multichannel analyzer (PMA-12).

A detailed description of the IPV characterization apparatus along with an in-depth explanation of the calibration process for the corresponding indoor light powers are provided in the Supporting Information Section C and elsewhere.^[84]

Figure 3c shows the J - V curve of a 500 nm thick $\text{FA}_{0.85}\text{Cs}_{0.15}\text{Pb}(\text{I}_{0.6}\text{Br}_{0.4})_3$ perovskite champion device with SAM + ImBr in the aforementioned device configuration (see Figure 3b). The J - V curve was measured under AM1.5G illumination conditions in both forward (dashed line) and reverse (solid line) scan directions. Details of the J - V measurement are provided in Supporting Information, Section A. The $\text{FA}_{0.85}\text{Cs}_{0.15}\text{Pb}(\text{I}_{0.6}\text{Br}_{0.4})_3$ with SAM + ImBr device exhibits a PCE of 15.5 %, a V_{oc} of 1.25 V, a short-circuit current density (J_{sc}) of 16.33 mA cm^{-2} , and a fill factor (FF) of 76.5% under AM1.5G conditions. The inset shows the EQE_{PV} plotted as a function of wavelength, where a maximum EQE of ≈ 0.78 was achieved. The device statistics of photovoltaic parameters are provided in Figure S13, Supporting Information.

The bandgap of the $\text{FA}_{0.85}\text{Cs}_{0.15}\text{Pb}(\text{I}_{0.6}\text{Br}_{0.4})_3$ perovskite was determined using the first derivative of the EQE_{PV} and it was found to be $E_g \approx 1.79 \text{ eV}$ and thus close to the optimum bandgap energy according to the detailed balance analysis in Figure 1b (see also Supporting Information Section D). IPV measurements were conducted on the same perovskite device using our setup as described above. Here, the incident light intensity was stepwise

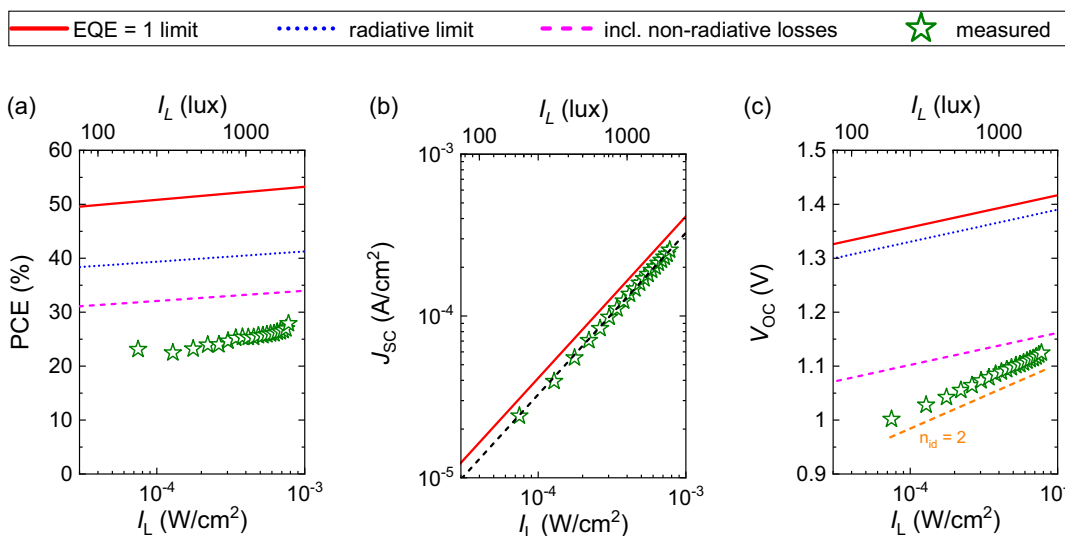


Figure 4. a) PCE of a $\text{FA}_{0.85}\text{Cs}_{0.15}\text{Pb}(\text{I}_{0.6}\text{Br}_{0.4})_3$ PPV device with Me-4PACz + ImBr plotted as a function of incident light intensity. While symbols are experimental data, the red solid line corresponds to the thermodynamic limit, the blue dotted line marks the upper radiative limit, and the purple dashed line identifies the upper limit including NR losses (estimated from AM1.5G conditions). b) Repetition of panel (a), but short-circuit current density (J_{sc}) plotted as a function of incident light intensity. c) Repetition of panel (a), but open-circuit voltage (V_{oc}) plotted as a function of incident light intensity. The orange dashed line is a guide to the eye corresponding to an ideality factor of $n_{id} = 2$.

varied between 150 and 1500 lux covering different indoor light scenarios (e.g., office with/without natural light, or a covered walkway^[9]); all J - V curves are shown in Figure S12, Supporting Information. **Figure 4a–c** shows the PCE, J_{sc} and V_{oc} (symbols), as obtained from the J - V curves, plotted as a function of light intensity, respectively. The PV parameters, as obtained at 185, 1000, and 2000 lux are shown in **Table 1**. For comparison, the calculated detailed balance limit in the case of an idealized unit step-function at a bandgap of 1.8 eV (red solid line), radiative (blue dotted line), and upper realistic (i.e., including NR losses; purple dashed line) limits are included. As shown in Figure 4c, the NR loss of the V_{oc} increases from approximately 130 mV (at 2000 lux) to 240 mV (at 185 lux) with decreasing irradiance. The corresponding expected upper limit of the PCE, as calculated based on the measured EQE_{PV} , for this system is 41%, with a V_{oc} of 1.36 V and a J_{sc} of 0.104 mA cm^{-2} (see blue star symbols in Figure 2b–d).

We further note that the experimentally obtained V_{oc} versus light intensity data follow an ideality factor $n_{id} = 2$ behavior (see orange dashed line in Figure 4c) indicative of the presence of Shockley–Read–Hall (SRH) recombination in the given intensity regime. From this, we can conclude that interface

recombination, which would result in n_{id} below 2 approaching unity, has been suppressed with the introduction of SAM and ImBr, to such an extent that bulk SRH recombination prevails as the dominant NR loss channel.^[85] To further support these findings and investigate the effect of SRH recombination on device performance under indoor lighting, we conducted one-dimensional DD simulations. The model assumes an active layer device thickness of 500 nm with a relative permittivity of $\epsilon = 24$ and an electrical energy bandgap of $E_g = 1.8 \text{ eV}$. The (radiative) bimolecular recombination coefficient in the active layer is estimated based on the radiative limit of the V_{oc} . Furthermore, we assumed ideal contacts and transport layers (i.e., no surface or interface recombination) with the dominant NR recombination mechanism to be trap-assisted recombination via mid-gap states in the bulk of the active layer. Detailed information on the DD model is provided elsewhere;^[86–88] the input DD model parameters are summarized in Table S1, Supporting Information.

Figure 5a–c shows the simulated PCE, J_{sc} and V_{oc} as a function of light intensity for the case of mid-gap traps having different SRH lifetimes, $\tau_{SRH} = \tau_n + \tau_p$ where τ_n and τ_p denote the electron and hole lifetimes, respectively. For comparison,

Table 1. PV parameters, such as open-circuit voltage (V_{oc}), short-circuit current density (J_{sc}), and PCE, for the wide-bandgap PPV, as experimentally obtained under different indoor light (Prizmatix 4000 K) irradiances. For comparison, PV parameters, as obtained from J - V curves under artificial AM1.5G conditions, are included. NR V_{oc} - and PCE losses are provided in brackets. The illuminance values (185, 1000, and 2000 lux) are selected based on literature.^[9]

Irradiance PV parameters	185 [lux] (indoor light e.g., office with no natural light ^[9])	1000 [lux] (e.g., office with natural light)	2000 [lux] (e.g., covered walkway)	Artificial AM1.5G (1 sun)
V_{oc} in [V] (NR loss in [V])	1.01 (0.24)	1.09 (0.16)	1.12 (0.13)	1.25
J_{sc} in [mA cm^{-2}]	0.02	0.13	0.25	16.33
PCE in [%]	23.1	25.3	27.9	15.5

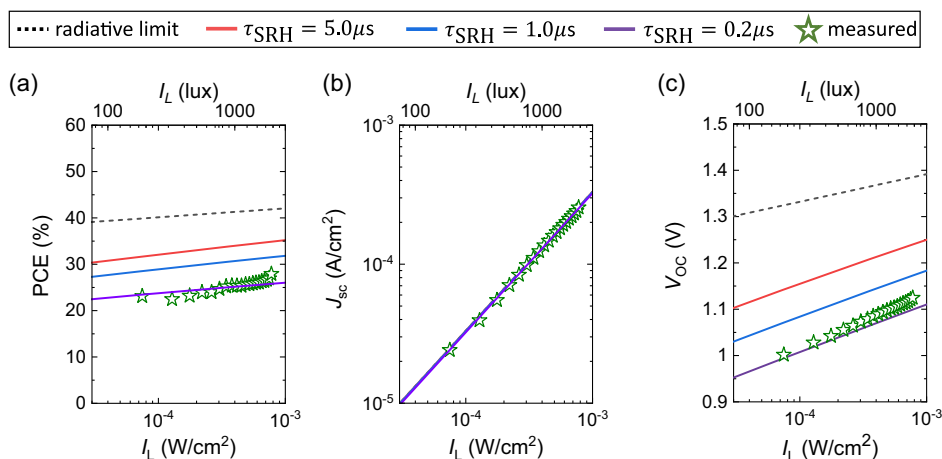


Figure 5. a) Simulated PCE, b) short-circuit current density (J_{sc}), and c) open-circuit voltage (V_{oc}) plotted against the incident light intensity and compared for different SRH lifetimes (τ_{SRH}). For comparison, the radiative limit (i.e., no trap-assisted recombination; black dashed line) and the experimental results (symbols), as obtained from light J - V measurement on the wide-bandgap PPV, have been included.

the radiative limit (i.e., no trap states; black dashed line) and our experimental results (symbols), as obtained from J - V measurements under indoor light, have been included. The simulated J - V curves of the different degrees of SRH recombination are provided in Figure S12, Supporting Information. Figure 5a-c shows that an increase in SRH lifetime, corresponding to a lower recombination rate, leads to enhanced V_{oc} and higher PCE. Notably, the case of $\tau_{SRH} = 0.2 \mu s$ coincides with our experimentally obtained PV parameters (symbols in Figure 4a-c) providing theoretical support for our above conclusion that SRH recombination is the main NR loss channel in the FA_{0.85}CS_{0.15}Pb(I_{0.6}Br_{0.4})₃ wide-bandgap PPV device. Furthermore, the DD simulation results demonstrate that a reduction of SRH recombination can enhance the PCE to get closer to its radiative limit. This finding is in line with ongoing endeavors in the PSC community to further advance the performance of inverted devices, which center around the reduction of the defect- and interface-recombination as well as optimization of charge transport.^[42,89-94] It is worth mentioning that most device optimization pathways for performance improvements are currently developed with respect to outdoor applications (i.e., typically under AM1.5G conditions). However, while some of

these approaches may be adapted for improving PSC performance under indoor conditions, further exploration of the links between fundamental device physics, overall efficiency, and engineering is required.^[95-97] In this context, the overall efficient charge transport in PSCs readily enables the preparation of thick-junction (i.e., >300 nm) and shunt-resistance-increased, high-efficient devices (as opposed to organic semiconductor-based solar cells^[98]), which is not only crucial requirement for device up-scaling but also a necessity for the commercialization of PSC for indoor applications.^[8]

7. Exemplification of a 2D Perovskite Device

We further investigated the use of 2D perovskites for IPV applications. Devices with the device architecture PTAA/PFN-Br/Perovskite/PCBM/BCP/Cu were fabricated to compare the performance of 2D (PEAI₂MA₄Pb₅I₁₆, $\langle n \rangle = 5$) and 3D (MAPbI₃) perovskite structures with similar bandgaps (details of the device fabrication are provided in the Supporting Information, Section A). **Figure 6** shows the figures of merit for the 2D

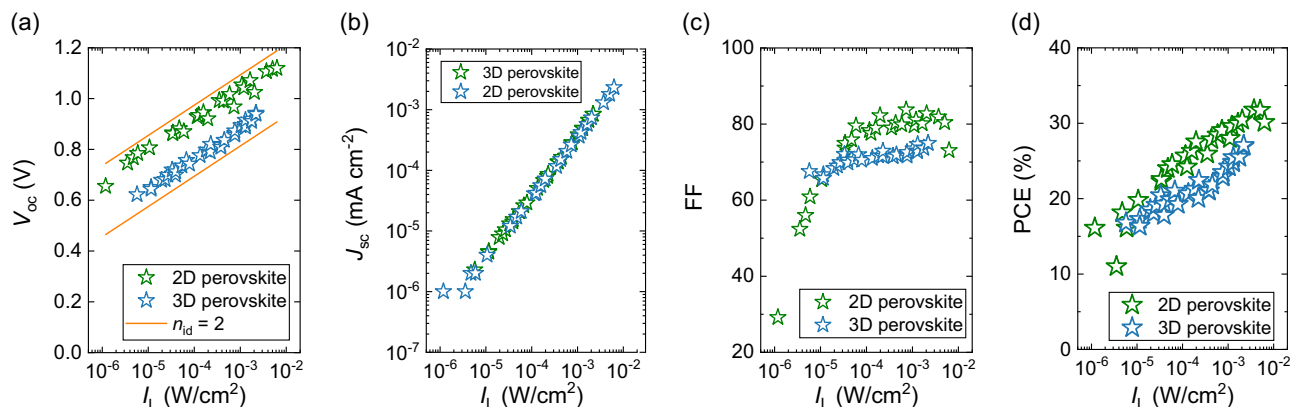


Figure 6. a) Open-circuit voltage (V_{oc}), b) short-circuit current density (J_{sc}), c) FF, and d) PCE plotted against the incident light intensity and compared for a 2D (green symbols) and 3D (blue symbols) PPV. The orange solid lines in panel (a) are guides to the eye corresponding to an ideality factor of $n_{id} = 2$.

(green symbols) and 3D (blue symbols) following the IPV characterization methods described above.

Although the 2D PSC demonstrated a higher V_{oc} (see Figure 6a) in comparison with the 3D PSC counterpart system, both devices exhibit similar J_{sc} (see Figure 6b). The superior overall performance of the 2D PSC (see Figure 6d) can be attributed to both the enhanced V_{oc} and FF (see Figure 6c) of the 2D PSC system when compared to the 3D PSC device – an observation that is consistent with the reduced interfacial losses described in previous reports.^[99–101]

8. Benchmarking and IPV Performance Prediction from Literature Data

In the absence of an established measurement condition with which to compare IPV devices, care must be taken when comparing IPV performance reports. To contextualize the exemplary device shown in this work, its performance was compared with a handful of the thousands of PPV devices stored in an open-access database.^[70] From the corresponding peer-reviewed articles, the AM1.5G open-circuit voltages and EQE_{PV} spectra were extracted. As summarized in Figure 7, these quantities were reanalyzed to predict IPV device performance under illumination from a 1000 lux LED-B4 source using a computational tool, *Indoor Extractor*, assuming a NR limit in this case. The code is additionally useful in considering superpositions of spectra, for example, to estimate performance under a mix of artificial light and sunlight incident through a window.

A description of the reanalysis process is provided in the Supporting Information, Section D, and a more comprehensive background is reported elsewhere.^[20] For comparison, the detailed balance limit for a maximum above-gap EQE of 1 (red solid line) and 0.85 (black dashed line) are added. It becomes clear that PPV performances under indoor illumination are,

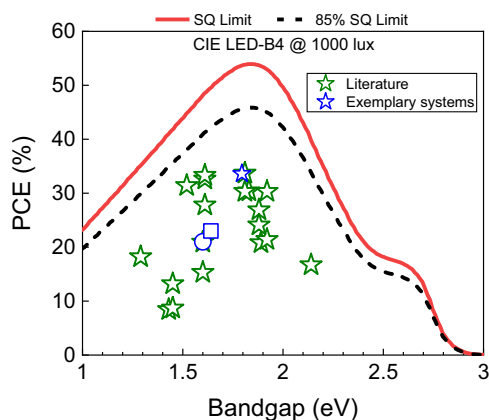


Figure 7. Comparison of PCE of PPV under indoor illumination (LED-B4 input spectrum at 1000 lux), as obtained by reanalyzing EQE_{PV} data taken from literature (green star symbols), plotted against the corresponding bandgap energy. For comparison, the radiative PCE limit in the detailed balance limit assuming above-gap EQE of 1 (red solid line) and 0.85 (black dashed line) are added. The blue star symbol marks the $FA_{0.85}CS_{0.15}Pb(I_{0.6}Br_{0.4})_3$ PPV with SAM + ImBr HTL studied in this work; blue circle (square) symbol corresponds to the 3D (2D) perovskite.

currently, still well below their predicted radiative detailed balance limits.

For comparison, the bandgap-optimized $FA_{0.85}CS_{0.15}Pb(I_{0.6}Br_{0.4})_3$ PPV with SAM and ImBr (blue star symbol) along the 3D MAPI (blue square symbol) and 2D (blue circle symbol) are added (see Figure 7). The former shows one of the highest efficiency (under LED-B4 spectrum) among the perovskite devices having an indoor-optimal bandgap of $\approx 1.7 - 1.9$ eV. As suggested by our DD simulations, a further reduction of trap-assisted recombination could help to minimize NR losses, enhance the PV performance under indoor illumination, and push the boundaries of indoor PCEs closer to their radiative limits.

9. Future Prospects for IPV Development

Rapid progress in PPVs for solar applications has been demonstrated since their first reports, due in part to innovations in transport layers, composition, and cell structure.^[102–105] The wider bandgaps which are optimal for IPV applications can be achieved via the compositional tuneability of perovskite materials. Tuning the Br content of halide perovskites has been demonstrated as one effective method of producing wider bandgap PPVs for IPV applications in this work and other recent reports.^[33,106]

High Br-containing PPV devices have associated issues including phase separation.^[106] Various reports have investigated methods of suppressing this effect, including surface passivation, hole transport material optimization, crystal size optimization, and alloying cations in the perovskite lattice.^[97,106–109] Light-induced halide segregation attributed to strain effects has been investigated and strain-releasing strategies have been established, including the addition of potassium iodide (KI)^[110] or the inclusion of Cl in a triple-halide composition.^[111] Due to their low formation energy, Br vacancies (V_{Br}) can be the dominant defects in Br-rich wide-bandgap PPV devices.^[112] Suppression of V_{Br} using KI treatment of defects has been suggested as a means of reducing NR recombination in wide-bandgap PPV devices for IPV applications.^[33]

To enhance the efficiency of IPV, it is crucial to minimize losses at the interfaces between different layers of the device.^[100] This can be achieved not only by improving material properties but also by optimizing interlayers and device structures. Another promising approach for IPV applications is the use of 2D perovskites, which appear to have substantially reduced transport limitations. By reducing V_{oc} losses and enhancing device lifetime, 2D and 2D/3D PPV systems show similar benefits as those obtained via interface engineering.^[99]

10. Conclusion

Given the nexus of developments in low-power electronics, wireless communications, big data, automation, and sensors, the inevitable rise of IPV will create new opportunities in fields such as IoT and wireless sensing. Considering their bandgap tunability and state of technological development from advances in tandem solar cells, perovskites are well-suited for use in IPV. However, there are several challenges that lay ahead. First,

measurement standardization will enable proper intercomparison between IPV devices and will illuminate the path toward highly efficient, stable devices. The exemplary results shown here emphasize the utility of measuring over a range of irradiances relevant to IPV applications to highlight avenues of device optimization. Second, the perovskite layer should not be understood in isolation. In contrast, the additional contribution of the transport layers to the overall operation of the device, including efficiency, stability, and durability, will be crucial to demonstrating technologically relevant devices. Finally, the field of IPV does not need to “reinvent the wheel” – given the vast literature on perovskite photovoltaics, approaches, and materials can be re-evaluated in the context of indoor conditions, for example, using the computational tool outlined here.

Supporting Information

Supporting Information is available from the Wiley Online Library or from the author.

Acknowledgements

This work was funded through the Welsh Government's Sêr Cymru II Program “Sustainable Advanced Materials” (Welsh European Funding Office – European Regional Development Fund). P.M. is a Sêr Cymru II Research Chair funded through the Welsh Government's Sêr Cymru II “Sustainable Advanced Materials” Program (European Regional Development Fund, Welsh European Funding Office, and Swansea University Strategic Initiative). This work was also funded by the UKRI through the EPSRC Program Grant EP/T028513/1 Application Targeted and Integrated Photovoltaics and the Centre for Integrative Semiconductor Materials (UKRI Research Partnership Investment Fund). The authors wish to thank George Koutsourakis and James C Blakesley from the National Physical Laboratory (NPL, UK) for fruitful discussions.

Conflict of Interest

The authors declare no conflict of interest.

Keywords

ambient photovoltaics, indoor photovoltaics, perovskite photovoltaics, testing

Received: March 1, 2024
Published online:

- [1] M. A. Iqbal, S. Hussain, H. Xing, M. A. Imran, in *Enabling the Internet of Things: Fundamentals, Design, and Applications*, Wiley-IEEE Press, 2021.
- [2] C. Polyzoidis, K. Rogdakis, E. Kymakis, *Adv. Energy Mater.* **2021**, *11*, 2101854.
- [3] K. L. Wang, Y. H. Zhou, Y. H. Lou, Z. K. Wang, *Chem. Sci.* **2021**, *12*, 11936.
- [4] I. Mathews, S. N. Kantareddy, T. Buonassisi, I. M. Peters, *Joule* **2019**, *3*, 1415.
- [5] X. Hou, Y. Wang, H. K. H. Lee, R. Datt, N. Uslar Miano, D. Yan, M. Li, F. Zhu, B. Hou, W. C. Tsoi, Z. Li, *J. Mater. Chem. A* **2020**, *8*, 21503.

- [6] S. Das, E. Mao, *Sustainable Energy Grids Networks* **2020**, *24*, 100408.
- [7] G. Burwell, O. J. Sandberg, W. Li, P. Meredith, M. Carnie, A. Armin, *Sol. RRL* **2022**, *6*, 2200315.
- [8] S. K. Thomas, A. Pockett, K. Seunarine, M. Spence, D. Raptis, S. Meroni, T. Watson, M. Jones, M. J. Carnie, *IoT* **2022**, *3*, 109.
- [9] W. Shockley, H. J. Queisser, *J. Appl. Phys.* **2004**, *32*, 510.
- [10] M. F. Müller, M. Freunek, L. M. Reindl, *IEEE J. Photovoltaics* **2013**, *3*, 59.
- [11] H. K. H. Lee, J. Barbé, W. C. Tsoi, in *Solar Cells and Light Management: Materials, Strategies and Sustainability*, Elsevier, Amsterdam, NL **2019**, pp. 355–388.
- [12] A. Al-Ashouri, E. Köhnen, B. Li, A. Magomedov, H. Hempel, P. Caprioglio, J. A. Márquez, A. B. M. Vilches, E. Kasparavicius, J. A. Smith, N. Phung, D. Menzel, M. Grischek, L. Kegelmann, D. Skroblin, C. Gollwitzer, T. Malinauskas, M. Jošt, G. Matič, B. Rech, R. Schlatmann, M. Topič, L. Korte, A. Abate, B. Stannowski, D. Neher, M. Stollerfoht, T. Unold, V. Getautis, S. Albrecht, *Science* **2020**, *370*, 1300.
- [13] W. Chen, Y. Zhu, J. Xiu, G. Chen, H. Liang, S. Liu, H. Xue, E. Birgersson, J. W. Ho, X. Qin, J. Lin, R. Ma, T. Liu, Y. He, A. M. C. Ng, X. Guo, Z. He, H. Yan, A. B. Djurišić, Y. Hou, *Nat. Energy* **2022**, *7*, 229.
- [14] S. Mazumdar, Y. Zhao, X. Zhang, *Sci. China Phys. Mech. Astron.* **2023**, *66*, 217304.
- [15] O. Almora, D. Baran, G. C. Bazan, C. I. Cabrera, S. Erten-Ela, K. Forberich, F. Guo, J. Hauch, A. W. Y. Ho-Baillie, T. J. Jacobsson, R. A. J. Janssen, T. Kirchartz, N. Kopidakis, M. A. Loi, R. R. Lunt, X. Mathew, M. D. McGehee, J. Min, D. B. Mitzi, M. K. Nazeeruddin, J. Nelson, A. F. Nogueira, U. W. Paetzold, B. P. Rand, U. Rau, H. J. Snaith, E. Unger, L. Vaillant-Roca, C. Yang, H. L. Yip, et al., *Adv. Energy Mater.* **2023**, *13*, 2102526.
- [16] S. Zeiske, W. Li, P. Meredith, A. Armin, O. J. Sandberg, *Cell Rep. Phys. Sci.* **2022**, *3*, 101096.
- [17] Y. Cui, L. Hong, T. Zhang, H. Meng, H. Yan, F. Gao, J. Hou, *Joule* **2021**, *5*, 1016.
- [18] D. Lübke, P. Hartnagel, J. Angona, T. Kirchartz, *Adv. Energy Mater.* **2021**, *11*, 2101474.
- [19] A. M. Kay, M. E. Fitzsimons, G. Burwell, P. Meredith, A. Armin, O. J. Sandberg, *Sol. RRL* **2023**, *7*, 2300277.
- [20] I. Fryc, S. W. Brown, Y. Ohno, in *Fifth Int. Conf. on Solid State Lighting*, Wiley-IEEE Press, San Diego, CA **2005**, p. 594111.
- [21] S. W. Brown, *Opt. Eng.* **2005**, *44*, 111309.
- [22] S. W. Brown, C. Santana, G. P. Eppeldauer, *J. Res. Natl. Inst. Stand. Technol.* **2002**, *107*, 363.
- [23] U. Rau, R. Brendel, *J. Appl. Phys.* **1998**, *84*, 6412.
- [24] Y. Peng, T. N. Huq, J. Mei, L. Portilla, R. A. Jagt, L. G. Occhipinti, J. L. MacManus-Driscoll, R. L. Z. Hoye, V. Pecunia, *Adv. Energy Mater.* **2021**, *11*, 2002761.
- [25] N. Lamminen, G. K. Grandhi, F. Fasulo, A. Hiltunen, H. Pasanen, M. Liu, B. Al-Anesi, A. Efimov, H. Ali-Löyty, K. Lahtonen, P. Mäkinen, A. Matuhina, A. B. Muñoz-García, M. Pavone, P. Vivo, *Adv. Energy Mater.* **2022**, *13*, 2203175.
- [26] L. K. Jagadamma, S. Wang, *Front. Chem.* **2021**, *9*, 632021.
- [27] A. Bulloch, S. Wang, P. Ghosh, L. K. Jagadamma, *Philos. Trans. R. Soc., A* **2022**, *380*, 20210144.
- [28] Z. Li, J. Zhang, S. Wu, X. Deng, F. Li, D. Liu, C. C. Lee, F. Lin, D. Lei, C. C. Chueh, Z. Zhu, A. K. Y. Jen, *Nano Energy* **2020**, *78*, 105377.
- [29] C. H. Chen, Z. H. Su, Y. H. Lou, Y. J. Yu, K. L. Wang, G. L. Liu, Y. R. Shi, J. Chen, J. J. Cao, L. Zhang, X. Y. Gao, Z. K. Wang, *Adv. Mater.* **2022**, *34*, e2200320.
- [30] H. K. H. Lee, J. Barbé, S. M. P. Meroni, T. Du, C. T. Lin, A. Pockett, J. Troughton, S. M. Jain, F. De Rossi, J. Baker, M. J. Carnie,

- M. A. McLachlan, T. M. Watson, J. R. Durrant, W. C. Tsoi, *Sol. RRL* **2019**, *3*, 1800207.
- [31] M. J. Wu, C. C. Kuo, L. S. Jhuang, P. H. Chen, Y. F. Lai, F. C. Chen, *Adv. Energy Mater.* **2019**, *9*, 1901863.
- [32] C. Zhang, C. Liu, Y. Gao, S. Zhu, F. Chen, B. Huang, Y. Xie, Y. Liu, M. Ma, Z. Wang, S. Wu, R. E. I. Schropp, Y. Mai, *Adv. Sci.* **2022**, *9*, 2204138.
- [33] G. Lucarelli, F. Di Giacomo, V. Zardetto, M. Creatore, T. M. Brown, *Nano Res.* **2017**, *10*, 2130.
- [34] L. K. Jagadamma, O. Blaszczyk, M. T. Sajjad, A. Ruseckas, I. D. W. Samuel, *Sol. Energy Mater. Sol. Cells* **2019**, *201*, 110071.
- [35] F. Di Giacomo, V. Zardetto, G. Lucarelli, L. Cinà, A. Di Carlo, M. Creatore, T. M. Brown, *Nano Energy* **2016**, *30*, 460.
- [36] J. Xu, J. Xi, H. Dong, N. Ahn, Z. Zhu, J. Chen, P. Li, X. Zhu, J. Dai, Z. Hu, B. Jiao, X. Hou, J. Li, Z. Wu, *Nano Energy* **2021**, *88*, 106286.
- [37] W. F. Yang, J. J. Cao, J. Chen, K. L. Wang, C. Dong, Z. K. Wang, L. S. Liao, *Sol. RRL* **2021**, *5*, 2000800.
- [38] M. Lee, E. Choi, A. M. Soufiani, J. Lim, M. Kim, D. Chen, M. A. Green, J. Seidel, S. Lim, J. Kim, X. Dai, R. Lee-Chin, B. Zheng, Z. Hameiri, J. Park, X. Hao, J. S. Yun, *Adv. Funct. Mater.* **2021**, *31*, 2008908.
- [39] M. Li, C. Zhao, Z. K. Wang, C. C. Zhang, H. K. H. Lee, A. Pockett, J. Barbé, W. C. Tsoi, Y. G. Yang, M. J. Carnie, X. Y. Gao, W. X. Yang, J. R. Durrant, L. S. Liao, S. M. Jain, *Adv. Energy Mater.* **2018**, *8*, 1801509.
- [40] R. D. J. Oliver, P. Caprioglio, F. Peña-Camargo, L. R. V. Buizza, F. Zu, A. J. Ramadan, S. G. Motti, S. Mahesh, M. M. McCarthy, J. H. Warby, Y. H. Lin, N. Koch, S. Albrecht, L. M. Herz, M. B. Johnston, D. Neher, M. Stolterfoht, H. J. Snaith, *Energy Environ. Sci.* **2022**, *15*, 714.
- [41] P. Caprioglio, J. A. Smith, R. D. J. Oliver, A. Dasgupta, S. Choudhary, M. D. Farrar, A. J. Ramadan, Y. H. Lin, M. G. Christoforo, J. M. Ball, J. Diekmann, J. Thiesbrummel, K. A. Zaininger, X. Shen, M. B. Johnston, D. Neher, M. Stolterfoht, H. J. Snaith, *Nat. Commun.* **2023**, *14*, 932.
- [42] S. Zhang, R. Wu, C. Mu, Y. Wang, L. Han, Y. Wu, W. H. Zhu, *ACS Mater. Lett.* **2022**, *4*, 1976.
- [43] D. Zhang, H. Zhang, H. Guo, F. Ye, S. Liu, Y. Wu, *Adv. Funct. Mater.* **2022**, *32*, 2200174.
- [44] Y. R. Kim, O. J. Sandberg, S. Zeiske, G. Burwell, D. B. Riley, P. Meredith, A. Armin, *Adv. Funct. Mater.* **2023**, *33*, 2300147.
- [45] Y. Li, L. Meng, Y. Yang, G. Xu, Z. Hong, Q. Chen, J. You, G. Li, Y. Yang, Y. Li, *Nat. Commun.* **2016**, *7*, 10214.
- [46] G. Burwell, N. Burrridge, E. Bond, W. Li, P. Meredith, A. Armin, *Adv. Electron. Mater.* **2021**, *7*, 2100192.
- [47] X. Zhao, T. Liu, Y.-L. Loo, X. Zhao, T. Liu, Y.-L. Loo, *Adv. Mater.* **2022**, *34*, 2105849.
- [48] Y. Zhang, N. G. Park, *ACS Energy Lett.* **2022**, *7*, 757.
- [49] C. Liang, H. Gu, Y. Xia, Z. Wang, X. Liu, J. Xia, S. Zuo, Y. Hu, X. Gao, W. Hui, L. Chao, T. Niu, M. Fang, H. Lu, H. Dong, H. Yu, S. Chen, X. Ran, L. Song, B. Li, J. Zhang, Y. Peng, G. Shao, J. Wang, Y. Chen, G. Xing, W. Huang, *Nat. Energy* **2021**, *6*, 38.
- [50] Y. W. Jang, S. Lee, K. M. Yeom, K. Jeong, K. Choi, M. Choi, J. H. Noh, *Nat. Energy* **2021**, *6*, 63.
- [51] R. Azmi, E. Ugur, A. Seitkhan, F. Aljamaan, A. S. Subbiah, J. Liu, G. T. Harrison, M. I. Nugraha, M. K. Eswaran, M. Babics, Y. Chen, F. Xu, T. G. Allen, A. U. Rehman, C.-L. Wang, T. D. Anthopoulos, U. Schwingenschlögl, M. D. Bastiani, E. Aydin, S. D. Wolf, *Science* **2022**, *376*, 73.
- [52] J. H. Kim, C. M. Oh, I. W. Hwang, J. Kim, C. Lee, S. Kwon, T. Ki, S. Lee, H. Kang, H. Kim, K. Lee, *Adv. Mater.* **2023**, *35*, 2302143.
- [53] F. Zhang, S. Yeon Park, C. Yao, H. Lu, S. P. Dunfield, C. Xiao, S. Uličná, X. Zhao, L. Du Hill, X. Chen, X. Wang, L. E. Mundt, K. H. Stone, L. T. Schelhas, G. Teeter, S. Parkin, E. L. Ratcliff, Y.-L. Loo, J. J. Berry, M. C. Beard, Y. Yan, B. W. Larson, K. Zhu, *Science* **2022**, *375*, 71.
- [54] M. Dessimoz, S. M. Yoo, H. Kanda, C. Igci, H. Kim, M. K. Nazeeruddin, *J. Phys. Chem. Lett.* **2021**, *12*, 11323.
- [55] R. B. Cevallos-Toledo, I. Rosa-Pardo, R. Arenal, V. Oestreicher, M. Fickert, G. Abellán, R. E. Galian, J. Pérez-Prieto, *Angew. Chem., Int. Ed.* **2021**, *60*, 27312.
- [56] H. Tsai, W. Nie, J. C. Blancon, C. C. Stoumpos, C. M. M. Soe, J. Yoo, J. Crochet, S. Tretiak, J. Even, A. Sadhanala, G. Azzellino, R. Brenes, P. M. Ajayan, V. Bulović, S. D. Stranks, R. H. Friend, M. G. Kanatzidis, A. D. Mohite, *Adv. Mater.* **2018**, *30*, 1704217.
- [57] J. Xu, Z. Ku, Y. Zhang, D. Chao, H. J. Fan, *Adv. Mater. Technol.* **2016**, *1*, 1600074.
- [58] T. Berestok, C. Diestel, N. Ortlieb, J. Buettner, J. Matthews, P. S. C. Schulze, J. C. Goldschmidt, S. W. Glunz, A. Fischer, *Sol. RRL* **2021**, *5*, 2100662.
- [59] S. Zeiske, P. Meredith, A. Armin, G. Burwell, *APL Energy* **2023**, *1*, 26103.
- [60] J. Thiesbrummel, V. M. Le Corre, F. Peña-Camargo, L. Perdígón-Toro, F. Lang, F. Yang, M. Grischek, E. Gutierrez-Partida, J. Warby, M. D. Farrar, S. Mahesh, P. Caprioglio, S. Albrecht, D. Neher, H. J. Snaith, M. Stolterfoht, *Adv. Energy Mater.* **2021**, *11*, 2101447.
- [61] V. M. Le Corre, J. Diekmann, F. Peña-Camargo, J. Thiesbrummel, N. Tokmoldin, E. Gutierrez-Partida, K. P. Peters, L. Perdígón-Toro, M. H. Futscher, F. Lang, J. Warby, H. J. Snaith, D. Neher, M. Stolterfoht, *Sol. RRL* **2022**, *6*, 2100772.
- [62] K. M. Anoop, M. V. Khenkin, F. Di Giacomo, Y. Galagan, S. Rahmany, L. Etgar, E. A. Katz, I. Visoly-Fisher, *Sol. RRL* **2020**, *4*, 1900335.
- [63] L. Rakocevic, F. Ernst, N. T. Yimga, S. Vashishtha, T. Aernouts, T. Heumueller, C. J. Brabec, R. Gehlhaar, J. Poortmans, *Sol. RRL* **2019**, *3*, 1900338.
- [64] M. H. Ann, J. Kim, M. Kim, G. Alosaimi, D. Kim, N. Y. Ha, J. Seidel, N. Park, J. S. Yun, J. H. Kim, *Nano Energy* **2020**, *68*, 104321.
- [65] J. Dagar, S. Castro-Hermosa, G. Lucarelli, F. Cacialli, T. M. Brown, *Nano Energy* **2018**, *49*, 290.
- [66] C. Teixeira, P. Spinelli, L. A. Castriotta, D. Müller, S. Öz, L. Andrade, A. Mendes, A. Di Carlo, U. Würfel, K. Wojciechowski, D. Forgács, *Adv. Funct. Mater.* **2022**, *32*, 2206761.
- [67] IEC TS 62607-7-2:2023 ED1 Nanomanufacturing – Key Control Characteristics – Part 7-2: Nano-Enabled Photovoltaics-Device Evaluation Method for Indoor Light, **2023**.
- [68] M. Saliba, E. Unger, L. Etgar, J. Luo, T. J. Jacobsson, *Nat. Commun.* **2023**, *14*, 5445.
- [69] T. J. Jacobsson, A. Hultqvist, A. García-Fernández, A. Anand, A. Al-Ashouri, A. Hagfeldt, A. Crovetto, A. Abate, A. G. Ricciardulli, A. Vijayan, A. Kulkarni, A. Y. Anderson, B. P. Darwich, B. Yang, B. L. Coles, C. A. R. Perini, C. Rehermann, D. Ramirez, D. Fairen-Jimenez, D. Di Girolamo, D. Jia, E. Avila, E. J. Juarez-Perez, F. Baumann, F. Mathies, G. S. A. González, G. Boschloo, G. Nasti, G. Paramasivam, G. Martínez-Denegri, et al., *Nat. Energy* **2022**, *7*, 107.
- [70] N. Zarrabi, O. J. Sandberg, S. Zeiske, W. Li, D. B. Riley, P. Meredith, A. Armin, *Nat. Commun.* **2020**, *11*, 5567.
- [71] E. Unger, T. J. Jacobsson, *ACS Energy Lett.* **2022**, *7*, 1240.
- [72] Z. Zhang, H. Wang, T. J. Jacobsson, J. Luo, *Nat. Commun.* **2022**, *13*, 7639.
- [73] J. Zhang, B. Liu, Z. Liu, J. Wu, S. Arnold, H. Shi, T. Osterrieder, J. A. Hauch, Z. Wu, J. Luo, J. Wagner, C. G. Berger, T. Stubhan, F. Schmitt, K. Zhang, M. Sytnyk, T. Heumueller, C. M. Sutter-Fella, I. M. Peters, Y. Zhao, C. J. Brabec, *Adv. Energy Mater.* **2023**, *13*, 2302594.
- [74] T. Osterrieder, F. Schmitt, L. Lüer, J. Wagner, T. Heumueller, J. Hauch, C. J. Brabec, *Energy Environ. Sci.* **2023**, *16*, 3984.

- [75] X. Du, L. Lüer, T. Heumueller, J. Wagner, C. Berger, T. Osterrieder, J. Wortmann, S. Langner, U. Vongsaysy, M. Bertrand, N. Li, T. Stubhan, J. Hauch, C. J. Brabec, *Joule* **2021**, 5, 495.
- [76] F. Laufer, S. Ziegler, F. Schackmar, E. A. Moreno Viteri, M. Götz, C. Debus, F. Isensee, U. W. Paetzold, *Sol. RRL* **2023**, 7, 2201114.
- [77] P. Calado, A. M. Telford, D. Bryant, X. Li, J. Nelson, B. C. O'Regan, P. R. F. Barnes, *Nat. Commun.* **2016**, 7, 13831.
- [78] N. E. Courtier, *Phys. Rev. Appl.* **2020**, 10, 24031.
- [79] J. Hüpkens, U. Rau, T. Kirchartz, *Sol. RRL* **2022**, 6, 2100720.
- [80] S. Zeiske, O. J. Sandberg, N. Zarrabi, W. Li, P. Meredith, A. Armin, *Nat. Commun.* **2021**, 12, 3603.
- [81] T. Kirchartz, L. Krückemeier, E. L. Unger, *APL Mater.* **2018**, 6, 100702.
- [82] R. Jose, S. Ramakrishna, *Appl. Mater. Today* **2018**, 10, 127.
- [83] S. Zeiske, P. Meredith, A. Armin, G. Burwell, *APL Energy* **2023**, 1, 026103.
- [84] P. Caprioglio, C. M. Wolff, O. J. Sandberg, A. Armin, B. Rech, S. Albrecht, D. Neher, M. Stollerfoht, *Adv. Energy Mater.* **2020**, 10, 2000502.
- [85] O. J. Sandberg, A. Sundqvist, M. Nyman, R. Österbacka, *Phys. Rev. Appl.* **2016**, 5, 044005.
- [86] T. S. Sherkar, C. Momblona, L. Gil-Escrig, H. J. Bolink, L. J. A. Koster, *Adv. Energy Mater.* **2017**, 7, 1602432.
- [87] O. J. Sandberg, J. Kurpiers, M. Stollerfoht, D. Neher, P. Meredith, S. Shoaee, A. Armin, *Adv. Mater. Interfaces* **2020**, 7, 1903.
- [88] X. Yang, D. Luo, Y. Xiang, L. Zhao, M. Anaya, Y. Shen, J. Wu, W. Yang, Y. H. Chiang, Y. Tu, R. Su, Q. Hu, H. Yu, G. Shao, W. Huang, T. P. Russell, Q. Gong, S. D. Stranks, W. Zhang, R. Zhu, *Adv. Mater.* **2021**, 33, 2006435.
- [89] S. Wu, J. Zhang, Z. Li, D. Liu, M. Qin, S. H. Cheung, X. Lu, D. Lei, S. K. So, Z. Zhu, A. K. Y. Jen, *Joule* **2020**, 4, 1248.
- [90] H. Wang, P. Wang, Y. Sun, C. Gao, W. Miao, D. Li, Y. Yang, T. Wang, D. Liu, *Adv. Funct. Mater.* **2022**, 32, 2200331.
- [91] F. Ye, S. Zhang, J. Warby, J. Wu, E. Gutierrez-Partida, F. Lang, S. Shah, E. Saglamkaya, B. Sun, F. Zu, S. Shoaee, H. Wang, B. Stiller, D. Neher, W. H. Zhu, M. Stollerfoht, Y. Wu, *Nat. Commun.* **2022**, 13, 7454.
- [92] Z. Li, B. Li, X. Wu, S. A. Sheppard, S. Zhang, D. Gao, N. J. Long, Z. Zhu, *Science* **2022**, 376, 416.
- [93] S. Zhang, F. Ye, X. Wang, R. Chen, H. Zhang, L. Zhan, X. Jiang, Y. Li, X. Ji, S. Liu, M. Yu, F. Yu, Y. Zhang, R. Wu, Z. Liu, Z. Ning, D. Neher, L. Han, Y. Lin, H. Tian, W. Chen, M. Stollerfoht, L. Zhang, W. H. Zhu, Y. Wu, *Science* **2023**, 380, 404.
- [94] K. T. Mularso, J. Y. Jeong, G. S. Han, H. S. Jung, *Nanomaterials* **2023**, 13, 259.
- [95] Z. Guo, A. K. Jena, I. Takei, M. Ikegami, A. Ishii, Y. Numata, N. Shibayama, T. Miyasaka, *Adv. Funct. Mater.* **2021**, 31, 2103614.
- [96] M. Nyman, O. J. Sandberg, W. Li, S. Zeiske, R. Kerremans, P. Meredith, A. Armin, *Sol. RRL* **2021**, 5, 2100018.
- [97] A. A. Sutanto, P. Caprioglio, N. Drigo, Y. J. Hofstetter, I. Garcia-Benito, V. I. E. Quelo, D. Neher, M. K. Nazeeruddin, M. Stollerfoht, Y. Vaynzof, G. Grancini, *Chem* **2021**, 7, 1903.
- [98] J. D. Ziegler, K. Q. Lin, B. Meisinger, X. Zhu, M. Kober-Czerny, P. K. Nayak, C. Vona, T. Taniguchi, K. Watanabe, C. Draxl, H. J. Snaith, J. M. Lupton, D. A. Egger, A. Chernikov, *ACS Photonics* **2022**, 9, 3609.
- [99] E. von Hauff, *Chem* **2021**, 7, 1694.
- [100] M. A. Green, A. Ho-Baillie, H. J. Snaith, *Nat. Photonics* **2014**, 8, 506.
- [101] A. Kojima, K. Teshima, Y. Shirai, T. Miyasaka, *J. Am. Chem. Soc.* **2009**, 131, 6050.
- [102] H. S. Kim, C. R. Lee, J. H. Im, K. B. Lee, T. Moehl, A. Marchioro, S. J. Moon, R. Humphry-Baker, J. H. Yum, J. E. Moser, M. Grätzel, N. G. Park, *Sci. Rep.* **2012**, 2, 591.
- [103] M. M. Lee, J. Teuscher, T. Miyasaka, T. N. Murakami, H. J. Snaith, *Science* **2012**, 338, 643.
- [104] X. Wang, Y. Ling, X. Lian, Y. Xin, K. B. Dhungana, F. Perez-Orive, J. Knox, Z. Chen, Y. Zhou, D. Beery, K. Hanson, J. Shi, S. Lin, H. Gao, *Nat. Commun.* **2019**, 10, 695.
- [105] R. A. Belisle, K. A. Bush, L. Bertoluzzi, A. Gold-Parker, M. F. Toney, M. D. McGehee, *ACS Energy Lett.* **2018**, 3, 2694.
- [106] H. Zhang, X. Fu, Y. Tang, H. Wang, C. Zhang, W. W. Yu, X. Wang, Y. Zhang, M. Xiao, *Nat. Commun.* **2019**, 10, 1088.
- [107] M. Suri, A. Hazarika, B. W. Larson, Q. Zhao, M. Vallés-Pelarda, T. D. Siegler, M. K. Abney, A. J. Ferguson, B. A. Korgel, J. M. Luther, *ACS Energy Lett.* **2019**, 4, 1954.
- [108] Y. Zhao, P. Miao, J. Elia, H. Hu, X. Wang, T. Heumueller, Y. Hou, G. J. Matt, A. Osvet, Y. T. Chen, M. Tarragó, D. de Ligny, T. Przybilla, P. Denninger, J. Will, J. Zhang, X. Tang, N. Li, C. He, A. Pan, A. J. Meixner, E. Spiecker, D. Zhang, C. J. Brabec, *Nat. Commun.* **2020**, 11, 6328.
- [109] J. Xu, C. C. Boyd, Z. J. Yu, A. F. Palmstrom, D. J. Witter, B. W. Larson, R. M. France, J. Werner, S. P. Harvey, E. J. Wolf, W. Weigand, S. Manzoor, M. F. A. M. van Hest, J. J. Berry, J. M. Luther, Z. C. Holman, M. D. McGehee, *Science* **2020**, 367, 1097.
- [110] J. Kang, L. W. Wang, *J. Phys. Chem. Lett.* **2017**, 8, 489.
- [111] S. Mahesh, J. M. Ball, R. D. J. Oliver, D. P. McMeekin, P. K. Nayak, M. B. Johnston, H. J. Snaith, *Energy Environ. Sci.* **2020**, 13, 258.
- [112] P. Caprioglio, S. Caicedo-Dávila, T. C. J. Yang, C. M. Wolff, F. Peña-Camargo, P. Fiala, B. Rech, C. Ballif, D. Abou-Ras, M. Stollerfoht, S. Albrecht, Q. Jeangros, D. Neher, *ACS Energy Lett.* **2021**, 6, 419.